Title

Intravenous Ferumoxytol Allows Noninvasive MR Imaging Monitoring of Macrophage Migration into Stem Cell Transplants

Journal

Radiology, 264(3)

ISSN

0033-8419

Authors

Khurana, Aman
Nejadnik, Hossein
Gawande, Rakhee
et al.

Publication Date

2012-09-01

DOI

10.1148/radiol.12112393

Peer reviewed

Intravenous Ferumoxytol Allows Noninvasive MR Imaging Monitoring of Macrophage Migration into Stem Cell Transplants[1]

Aman Khurana, MD
Hossein Nejadnik, MD
Rakhee Gawande, MBBS
Guiting Lin, MD, PhD
Sungmin Lee, MS
Solomon Messing, MS
Rosalinda Castaneda, MS
Nikita Derugin, MA
Laura Pisani, PhD
Tom F. Lue, MD
Heike E. Daldrup-Link, MD, PhD

Purpose: To develop a clinically applicable imaging technique for monitoring differential migration of macrophages into viable and apoptotic matrix-associated stem cell implants (MASIs) in arthritic knee joints.

Materials and Methods: With institutional animal care and use committee approval, six athymic rats were injected with intravenous ferumoxytol (0.5 mmol iron per kilogram of body weight) to preload macrophages of the reticuloendothelial system with iron oxide nanoparticles. Forty-eight hours later, all animals received MASIs of viable adipose-derived stem cells (ADSCs) in an osteochondral defect of the right femur and mitomycin-pretreated apoptotic ADSCs in an osteochondral defect of the left femur. One additional control animal each received intravenous ferumoxytol and bilateral scaffold-only implants (without cells) or bilateral MASIs without prior ferumoxytol injection. All knees were imaged with a 7.0-T magnetic resonance (MR) imaging unit with T2-weighted fast spin-echo sequences immediately after, as well as 2 and 4 weeks after, matrix-associated stem cell implantation. Signal-to-noise ratios (SNRs) of viable and apoptotic MASIs were compared by using a linear mixed-effects model. MR imaging data were correlated with histopathologic findings.

Results: All ADSC implants showed a slowly decreasing T2 signal over 4 weeks after matrix-associated stem cell implantation. SNRs decreased significantly over time for the apoptotic implants (SNRs on the day of matrix-associated stem cell implantation, 2 weeks after the procedure, and 4 weeks after the procedure were 16.9, 10.9, and 6.7, respectively; $P = .0004$) but not for the viable implants (SNRs on the day of matrix-associated stem cell implantation, 2 weeks after the procedure, and 4 weeks after the procedure were 17.7, 16.2, and 15.7, respectively; $P = .2218$). At 4 weeks after matrix-associated stem cell implantation, SNRs of apoptotic ADSCs were significantly lower than those of viable ADSCs (mean, 6.7 vs 15.7; $P = .0013$). This corresponded to differential migration of iron-loaded macrophages into MASIs.

Conclusion: Iron oxide loading of macrophages in the reticuloendothelial system by means of intravenous ferumoxytol injection can be utilized to monitor differential migration of bone marrow macrophages into viable and apoptotic MASIs in a rat model.

Supplemental material: *http://radiology.rsna.org/lookup/suppl/doi:10.1148/radiol.12112393/-/DC1*

[1] From the Department of Radiology, Molecular Imaging Program at Stanford, Stanford University School of Medicine, 725 Welch Rd, Room 1665, Stanford, CA 94305-5654 (A.K., H.N., R.G., S.L., R.C., L.P., H.E.D.); Departments of Urology (G.L., T.F.L.) and Neurology (N.D.), University of California, San Francisco, San Francisco, Calif; and Departments of Electrical Engineering (S.L.) and Statistics and Communication (S.M.), Stanford University, Stanford, Calif. Received November 9, 2011; revision requested December 19; revision received March 16, 2012; accepted April 3; final version accepted April 19. **Address correspondence to** H.E.D. (e-mail: *H.E.Daldrup-Link@stanford.edu*).

Osteochondral defects caused by degenerative arthritis, inflammatory arthritis, or trauma represent a major cause of chronic joint pain and related disabilities in our society. The limited self-regeneration capacity of cartilage requires therapeutic approaches for joint restoration (1,2). Matrix-associated stem cell implants (MASIs) have a high potential for bone and cartilage regeneration (3,4). However, a major challenge of current approaches is death of the transplanted cells because of failed engraftment and/or immune rejection (5,6). In case of graft failure, the transplanted cells die first (eg, because of hypoxia or mechanical factors), which leads to secondary macrophage influx and clearance of dead cells (7). In case of graft rejection, specific stem cell immunophenotypes attract monocytes, macrophages, lymphocytes, and dendritic cells, which recognize, kill, and eliminate the transplanted cells (8).

These host immune responses to stem cell implants represent a major challenge for tissue engineering outcomes, especially as host immune responses refer to macrophage interactions with transplanted cells (9–12). Dupont et al (9) and Lyons et al (10) reported that host macrophages extensively migrated into stem cell implants in bone defects in rat models. Depending on underlying pro- or antiinflammatory physiologic conditions, the macrophage migration into MASIs could facilitate bone and cartilage remodeling (10,13) or counteract the engraftment process (10,14,15). In the majority of cases, the natural immunity to MASIs was not protective but instead led to clearance of transplanted cells from the implant (9,16). Transplants with a large quantity of apoptotic cells led to a release of chemoattractant factors, such as lysophosphatidylcholine, which induce a migration of bone marrow macrophages into MASIs to phagocytose the transplanted cells (17–19).

An imaging technique that could directly visualize macrophage migration into MASIs could serve as an imaging biomarker for host immune responses to matrix-associated stem cell implantation and could thereby help diagnose apoptotic transplants. We and other investigators have shown in preclinical and clinical investigations (20,21) that macrophages in bone marrow phagocytose intravenously administered ultrasmall superparamagnetic iron oxide (USPIO) nanoparticles. In addition, we have shown that iron oxide–labeled cells can be depicted in MASIs by using magnetic resonance (MR) imaging (22–25). On the basis of these previous observations, we hypothesized that it should be possible to detect the in vivo migration of iron oxide–loaded macrophages into MASIs by using MR imaging.

Thus, the purpose of this study was to develop a clinically applicable imaging technique for monitoring differential migration of macrophages into viable and apoptotic MASIs in arthritic knee joints. If successful, this imaging technique could serve as a novel potentially clinically applicable biomarker for host immune responses to transplanted cells and could help identify apoptotic implants soon after matrix-associated stem cell implantation.

Advances in Knowledge

- Intravenous injection of ferumoxytol leads to uptake and iron oxide labeling of macrophages in the reticuloendothelial system; MR imaging can be used to depict the migration of the labeled macrophages to stem cell transplants in vivo.
- MR imaging helped identify migration of iron oxide–labeled macrophages into apoptotic stem cell transplants but not into viable stem cell transplants.
- The described MR imaging approach can be used to detect host immune responses to apoptotic stem cell transplants.

Implication for Patient Care

- The approach presented of "preloading" macrophages with iron oxide nanoparticles for subsequent in vivo tracking of host immune responses is in principle clinically translatable through an "off-label" use of the U.S. Food and Drug Administration–approved iron supplement ferumoxytol.

Materials and Methods

Contrast Agent

Ferumoxytol (Feraheme; Advanced Magnetics, Cambridge, Mass) is an iron supplement that has been approved by the U.S. Food and Drug Administration for intravenous treatment of iron deficiencies (26). Ferumoxytol consists of USPIO nanoparticles with a mean hydrodynamic diameter of 30 nm. The nanoparticles are composed of an iron oxide core (mean diameter, 6.76 nm ± 0.41 [standard deviation]) and a semisynthetic carbohydrate coating of polyglucose sorbitol carboxymethylether. Ferumoxytol nanoparticles have an effect on signal intensity on T1- and T2-weighted MR images because of their r1 relaxivity of

Published online before print
10.1148/radiol.12112393 **Content code:** BQ

Radiology 2012; 264:803–811

Abbreviations:
ADSC = adipose-derived stem cell
DAB = diaminobenzidine
MASI = matrix-associated stem cell implant
RES = reticuloendothelial system
SNR = signal-to-noise ratio
USPIO = ultrasmall superparamagnetic iron oxide

Author contributions:
Guarantors of integrity of entire study, A.K., H.E.D.; study concepts/study design or data acquisition or data analysis/interpretation, all authors; manuscript drafting or manuscript revision for important intellectual content, all authors; manuscript final version approval, all authors; literature research, A.K., H.N., R.G., S.L., T.F.L., H.E.D.; experimental studies, A.K., H.N., R.G., G.L., S.L., R.C., N.D., L.P., T.F.L., H.E.D.; statistical analysis, H.N., S.M., L.P., T.F.L.; and manuscript editing, A.K., H.N., N.D., L.P., T.F.L., H.E.D.

Funding:
This research was supported by the National Institutes of Health (grant R01AR054458).

Potential conflicts of interest are listed at the end of this article.

See also Science to Practice in this issue.

15 $mM^{-1} \cdot sec^{-1}$ (15 $L \cdot mmol^{-1} \cdot sec^{-1}$) and r2 relaxivity of 89 $mM^{-1} \cdot sec^{-1}$ (89 $L \cdot mmol^{-1} \cdot sec^{-1}$) at 1.5 T (27).

Stem Cell Culture and Apoptosis Induction

Adipose-derived stem cells (ADSCs) were extracted and characterized (G.L. and T.F.L.) from male Sprague-Dawley rats (28). ADSCs were cultured in Dulbecco's modified Eagle's medium (Invitrogen, Carlsbad, Calif) supplemented with 10% fetal bovine serum (Invitrogen), 100 IU/mL penicillin, and 100 μg/mL streptomycin (Invitrogen) at 37°C in a humidified 5% CO_2 atmosphere. At 80%–90% confluency, the ADSCs were trypsinized and were either cultured further or used for experiments. Before transplantation into the joints of the animals, half of the cells underwent apoptosis induction with mitomycin C (Sigma-Aldrich, St Louis, Mo), as previously described (22,29). In brief, ADSCs were incubated with 0.5 mg mitomycin C per milliliter of serum-free media for 6 hours at standard cell culture condition. Cells were carefully washed three times with Dulbecco's phosphate-buffered saline (Invitrogen) and were used for the in vivo experiment. A SensoLyte Homogeneous AMC Caspase 3/7 Assay Kit (AnaSpec, Fremont, Calif) was used to quantify caspase production by mitomycin-treated cells by means of the Ac-DEVD-AMC substrate (22). Caspase 3/7 production induces cleavage of Ac-DEVD-AMC, which generates the fluorophore AMC, which can be detected at an excitation of 354 nm and an emission of 442 nm. The caspase assay was prepared by using standard protocols. In brief, cell extracts were prepared for mitomycin-treated cells, viable cells, and serum-free media–treated cells. The cell extracts were mixed with caspase substrate solution on a plate shaker for 60 seconds at 100–200 rpm. Caspase 3/7 production was measured on a plate reader as the relative fluorescent intensity at an excitation of 354 nm and an emission of 442 nm.

Animal Model and ADSC Implantation

The study was approved by the institutional animal care and use committee of Stanford University. We examined eight athymic female Harlan rats (mean weight, 131 g ± 6). Seven rats received intravenous injections of ferumoxytol at a dose of 0.5 mmol iron per kilogram of body weight. Forty-eight hours after ferumoxytol administration, six of these rats received ADSC implants, and one control rat received scaffold implants only. One additional control rat received ADSC implants but no intravenous contrast agent injection. Matrix-associated stem cell implantation surgeries were performed in sterile conditions and with isoflurane anesthesia by an animal surgeon (N.D., with 30 years of experience). A circular osteochondral defect (2 mm in diameter and 1.5 mm deep) was created in the intertrochlear groove of the femur by using a microdrill (Ideal, Sycamore, Ill). Six rats (previously injected with ferumoxytol) and one control rat (not injected with ferumoxytol) received implants of 7.5×10^5 viable ADSCs in an agarose scaffold in the defect of the right knee joint and 7.5×10^5 apoptotic ADSCs in an agarose scaffold in the defect of the left knee joint. The location and consistency of the implants was confirmed visually. One additional control rat (previously injected with ferumoxytol) received agarose scaffold implants without cells (Type VII agarose; Sigma-Aldrich) in defects in both knees. The skin incision was closed, and buprenorphine (0.05 mg/kg) was administered to control pain.

MR Imaging

All rats underwent three MR imaging studies performed with a 7.0-T animal MR imaging unit ("microSigna 7.0" collaboration between GE Healthcare [Waukesha, Wis] and Varian [Walnut Creek, Calif]). These studies were performed immediately after matrix-associated stem cell implantation and at 2 and 4 weeks after matrix-associated stem cell implantation. The control animal that was not injected with ferumoxytol was only imaged immediately after matrix-associated stem cell implantation. Animals were anesthetized with 1.5%–2.0% isoflurane and were placed in the supine position in a custom-built single-channel transmit-receive partial birdcage radiofrequency coil with an inner diameter of 2 cm. Sagittal MR images of both knee joints were obtained with fast spin-echo sequences with the following parameters: repetition time msec/echo time msec, 3000/30; field of view, 2.5 × 2.5 cm; matrix, 256 × 256 pixels; section thickness, 0.5 mm; and 16 acquisitions. The mean signal intensity (SI) of all MASIs and the SI of noise in air were measured in consensus by two postdoctoral research fellows (A.K. and H.N., with 5 and 6 years of medical training, respectively), who used regions of interest (ROIs) and Osirix software (Pixmeo, Geneva, Switzerland). For each knee joint, average SIs were calculated for three 8–10-pixel ROIs in each MASI and for two 30-pixel ROIs in the background in front of (ie, in the phase-encoding direction of) the MASI. The signal-to-noise ratio (SNR) was calculated as the SI of the transplant divided by the SI of noise.

Histopathologic Examination

Animals were sacrificed after the last MR imaging procedure, and knee joints were explanted, dissected, and placed in a fixative and decalcifier (Cal-Ex II; Fisher Scientific, Fair Lawn, NJ) for 5–8 days to fix and decalcify the tissue simultaneously. The specimens were dissected parasagittally, were dehydrated through graded alcohol washes, and were embedded in paraffin. Tissue slices (5 μm thick) on glass slides were stained with standard hematoxylin-eosin to define the morphology of the ADSC transplants and with Prussian blue diaminobenzidine (DAB) to localize iron oxides in MASIs. We performed additional immunostaining of the deparaffinized and formalin-fixed specimens, including anti-CD68 staining to localize macrophages in the MASIs and fluorescence in situ hybridization (Rat IDetect Chromosome Paint Probes; ID Labs Biotechnology, London, Ontario, Canada) against chromosome Y to evaluate the presence and viability of implanted ADSCs from male donors in female recipient rats.

Statistical Analyses

SNRs for the viable and apoptotic MASI groups were tested for significant differences over time by using a mixed linear model with a random effect for each rat knee (Table). SNRs for viable and apoptotic MASI groups were also compared at week 4 by using a *t* test. Differences in caspase production between mitomycin-treated cells and untreated cells were compared by using a *t* test. $P < .05$ was considered to indicate a significant difference, except for the SNR comparison at week 4, for which $P < .0033$ was considered to indicate a significant difference, in line with the Bonferroni correction.

SNR in MASIs over Time

Coefficient*	Estimate	Standard Error of Estimate	*t* Value	*P* Value
Intercept	17.522	1.196	14.647	<.001
Apoptotic implants	−0.894	1.692	−0.529	.597
Scaffold only	8.028	2.393	3.355	.001
Week (viable trend)	−0.500	0.409	−1.222	.222
Interaction between apoptotic and week	−2.058	0.579	−3.557	<.001
Interaction between scaffold and week	−3.775	0.818	−4.613	<.001
Knee random effect variance	1.889	1.374	...	...
Residual variance	8.038	2.835	...	...

Note.—The linear mixed model was fit by using lme4 (a software package for the R statistical programming language) by means of restricted maximum likelihood, with rat knee as a random effect. We inserted a random effect for each rat knee to account for the within-observation correlation over time. Knees could differ substantially for each rat, so the best modeling strategy was to model the variation between each knee as a random effect. The results are nearly identical when each rat rather than each knee was used as a random effect. The number of observations was 42, the number of groups was 14 (at three time points), the log likelihood was −100.575, the deviance was 201.150, the Akaike information criterion was 217.150, and the Bayesian information criterion was 231.051.

*Effects relative to baseline factor "viable."

Results

Caspase production was significantly higher in the mitomycin-treated cells than in the untreated cells ($P = .0052$) (Fig 1). Animals injected with ferumoxytol demonstrated markedly decreased bone marrow signal on T2-weighted MR images in comparison with the control animal that had not received any ferumoxytol injection (Fig 2), indicating reticuloendothelial system (RES) uptake and macrophage phagocytosis of ferumoxytol (Figs E1 and E2 [online]). All ADSC transplants in osteochondral defects demonstrated high T2 signal immediately after matrix-associated stem cell implantation (Fig 2). The T2 signal of apoptotic MASIs markedly decreased at subsequent follow-up studies (2 and 4 weeks after matrix-associated stem cell implantation), while the T2 signal of viable MASIs decreased only slightly (Fig 2). The control animal that had received intravenous ferumoxytol and implants of agarose scaffold only (without stem cells) also showed a marked decline in T2 signal 2 and 4 weeks after matrix-associated stem cell implantation, similar to that seen in apoptotic ADSC implants (Fig 2).

Mean SNRs of apoptotic cell transplants were 16.9, 10.9, and 6.7 on the day of matrix-associated stem cell implantation, 2 weeks after the procedure, and 4 weeks after the procedure, respectively. Conversely, mean SNRs of viable cell transplants were 17.7, 16.2, and 15.7 on the day of matrix-associated stem cell implantation, 2 weeks after the procedure, and 4 weeks after the procedure, respectively. The linear mixed-effects model revealed that SNR declined significantly over time for apoptotic implants ($P = .0004$ [Fig 3, Table]). There was no significant trend for viable implants ($P = .2218$). At 4 weeks after matrix-associated stem cell implantation, SNRs of apoptotic ADSCs were significantly lower than those of viable ADSCs ($P = .0013$).

Hematoxylin-eosin staining 4 weeks after matrix-associated stem cell implantation revealed engraftment of viable ADSCs in osteochondral defects,

Figure 1

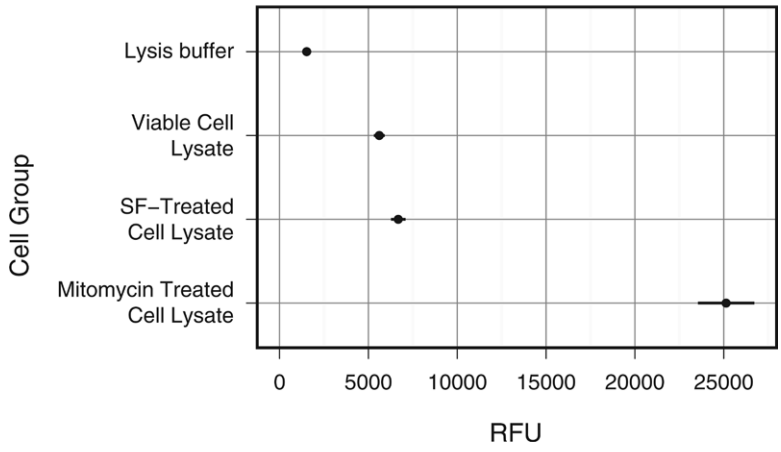

Figure 1: Graph shows relative fluorescence of viable serum-free media–treated cells and mitomycin-treated cells. Mitomycin-treated cells showed significant caspase production ($P < .01$). All data are means ± standard errors of the mean. *RFU* = relative fluorescence units, *SF* = serum-free media.

Figure 2

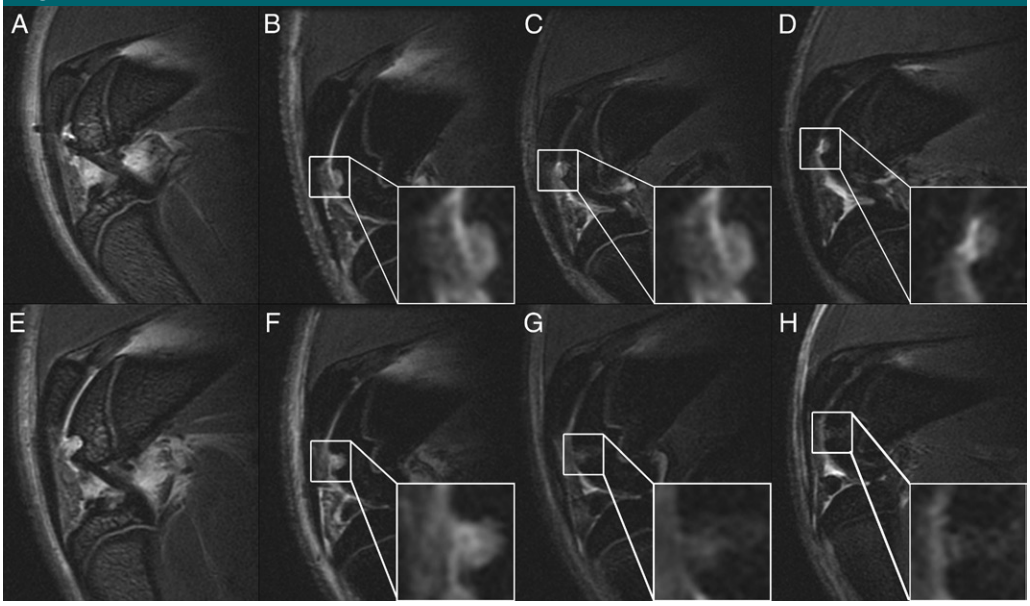

Figure 2: Sagittal T2-weighted fast spin-echo MR images (30/3000) of representative rat knees with viable MASIs (upper row) and apoptotic MASIs (lower row) in osteochondral defects, with zoomed insets of the implants. *A, E,* Images in control animal without ferumoxtyol injection, and, *B–D,* and, *F–H*, serial images in an animal that had been injected with ferumoxtyol 48 hours before matrix-associated stem cell implantation. Directly after matrix-associated stem cell implantation (week 0), the T2 signal of the viable implant (in *B*) and that of the apoptotic implant (in *F*) are not significantly different. However, follow-up images obtained 2 weeks (*C* and *G*) and 4 weeks (*D* and *H*) after matrix-associated stem cell implantation show a gradually decreasing T2 signal in apoptotic implants (*G* and *H*) but not in viable implants (*C* and *D*).

Figure 3

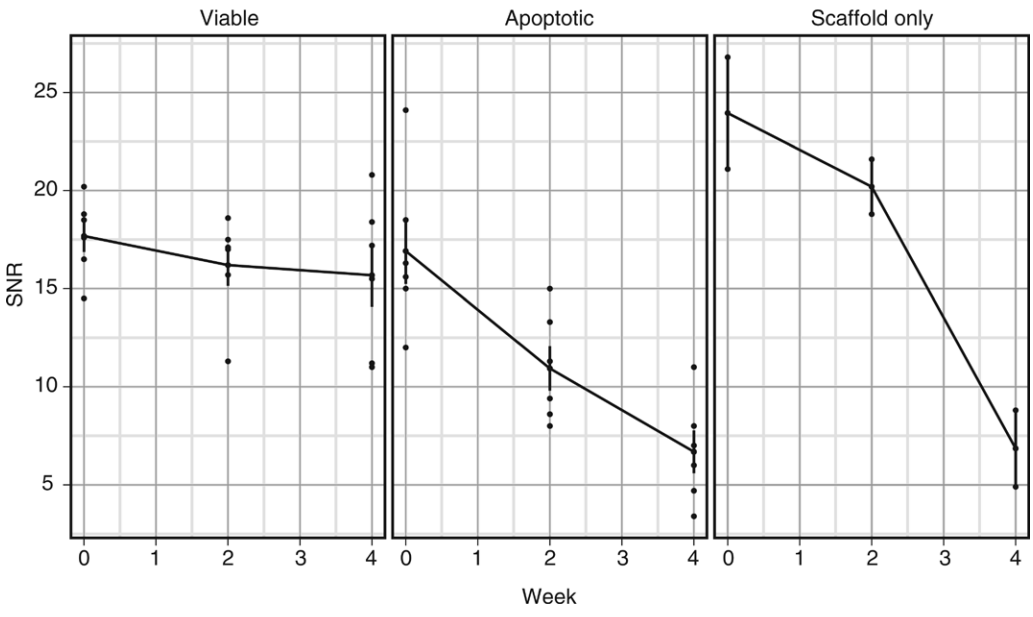

Figure 3: Graph shows SNRs of viable and apoptotic implants at different time points after matrix-associated stem cell implantation. Data are means and standard errors of mean for viable and apoptotic MASIs in six knee joints each and means for two knee joints with scaffold-only implants.

with remodeling of the joint surface. Conversely, apoptotic implants demonstrated persistent osteochondral defects (Fig 4, *A* and *B*). Prussian blue DAB staining revealed iron oxide particles in MASIs, with a relatively higher quantity of iron oxide particles in apoptotic MASIs than in viable MASIs (Fig 4, *C* and *D*). Anti-CD68 immunostaining revealed macrophages in both viable and apoptotic MASIs, with more abundant CD68-positive cells in apoptotic MASIs than in viable MASIs (Fig 4, *E* and *F*). To confirm the presence of implanted ADSCs from male donors in female rat recipients, fluorescence in situ hybridization against the Y chromosome was performed. It demonstrated Y-positive cells in viable MASIs but not in apoptotic MASIs (Fig 4, *G* and *H*).

Discussion

Our data demonstrated the feasibility of depicting host immune responses to stem cell transplants in vivo with MR imaging by preloading macrophages with intravenously administered ferumoxytol prior to stem cell transplantation. The presented macrophage tracking technique could help detect differential macrophage accumulation in viable versus apoptotic MASIs and could potentially also be applied in comparative investigations of macrophage responses to other stem cell transplants.

Our observations of macrophage migration into cell transplants are in accordance with findings by other investigators, who showed with postmortem histologic analyses that host macrophages migrate into MASIs in response to cell death and/or inflammatory reactions (9,14,15). Lyons et al (10) showed that macrophage migration also occurred into the scaffold only (without stem cells) in bone defects. On the other hand, evaluations by Arinzeh et al (30) confirmed that successful bone regeneration was not associated with marked immune responses. Compared with previously applied histopathologic evaluations, our MR imaging approach has the advantage of being noninvasive and applicable in vivo, thereby allowing close longitudinal evaluations of host immune responses in living subjects.

Figure 4

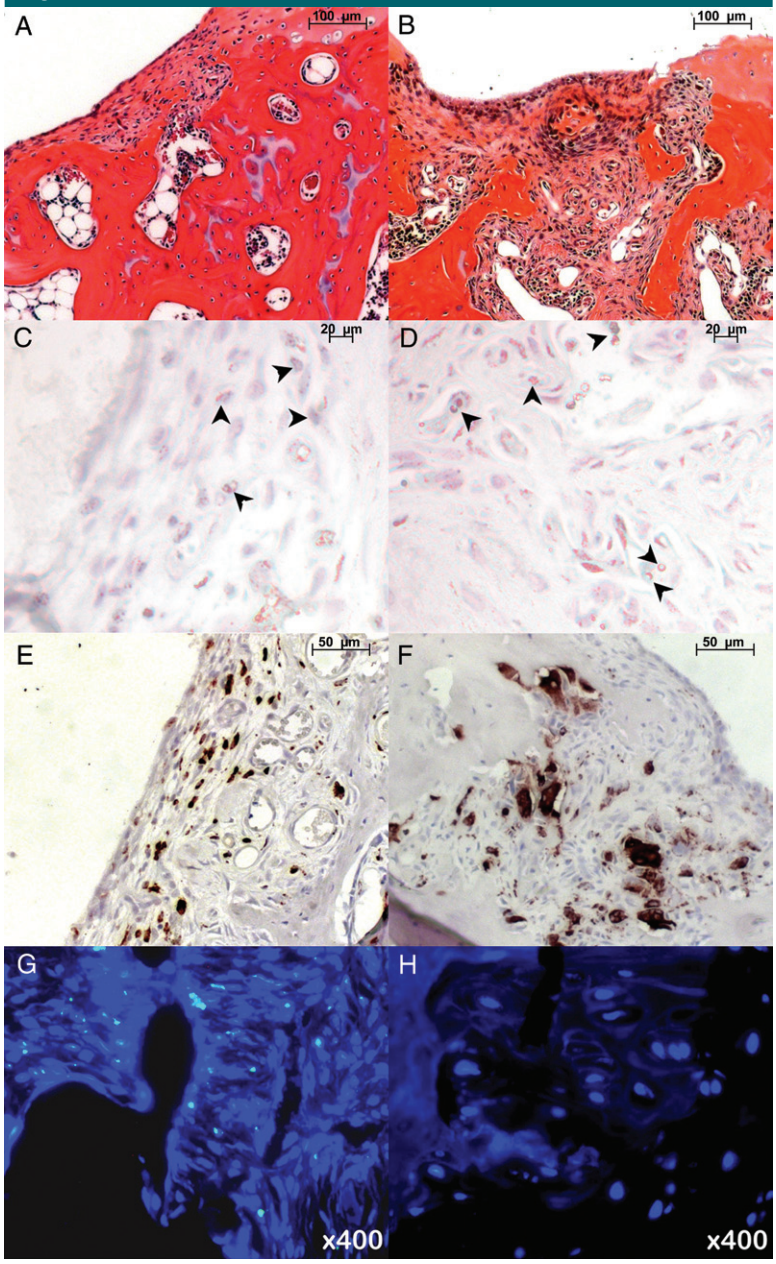

Figure 4: Histopathologic findings in osteochondral defects 4 weeks after matrix-associated stem cell implantation. *A, B,* Hematoxylin-eosin stains of, *A,* viable ADSC implant and, *B,* apoptotic ADSC implant in osteochondral defects. *C, D,* Prussian blue DAB stains show relatively more areas of iron (arrowheads) in, *D,* apoptotic implant than in, *C,* viable implant. *E, F,* Anti-CD68 staining shows more macrophages in, *F,* apoptotic implant than in, *E,* viable implant. *G, H,* Fluorescence in situ hybridization analysis shows presence of rat Y chromosome–positive cells in, *G,* viable MASI but not in, *H,* apoptotic MASI.

Intravenously administered USPIO nanoparticles have been applied extensively for MR imaging of macrophages in organs of the RES, such

as the liver (31,32), the spleen (31), lymph nodes (32,33), and bone marrow (34–36). The relatively large nanoparticles, which have a size on the order of plasma proteins, initially distribute in the blood pool, where they cause strong T1 and T2 relaxation time enhancement (37). The nanoparticles subsequently slowly extravasate across the sinusoids of microvessels in RES organs and accumulate in the interstitium, where they are slowly phagocytosed by macrophages. This process takes several hours (34,38). At 24 hours after injection, the persistent enhancement on T2-weighted MR images in RES organs corresponds to intracellular USPIO nanoparticles in macrophages at histopathologic examination (39,40). We chose to preload RES macrophages with the USPIO nanoparticle ferumoxytol 48 hours before planned stem cell transplantation to allow enough time for macrophage phagocytosis and to ensure minimal or no residual nanoparticles in the blood, considering a blood half-life of 67 minutes for ferumoxytol in rodents (21). This allowed subsequent tracking of labeled macrophages into unlabeled MASIs with MR imaging.

Our MR imaging approach could indirectly depict failed, apoptotic stem cell implants by depicting influx of iron-labeled macrophages into MASIs. This approach is closer to potential clinical applications than direct labeling of stem cells with iron oxides, as previously performed by our group and others (41–44). In addition, direct iron oxide labeling provided limited information about the viability of the transplanted cells (41).

We recognize the following limitations of our study: To ensure maximal RES preloading, we injected a higher dose of ferumoxytol into our animals (0.5 mmol iron per kilogram) than the usual ferumoxytol dose in patients (0.1 mmol iron per kilogram). Increased USPIO nanoparticle doses are recommended for rodent studies to compensate for the faster biodistribution in rodents than in humans (45). Of note, allergic reactions to ferumoxytol, presumably against the carboxymethyl dextran coating, have recently been described. Novel, third-generation iron oxide nanoparticles, which are also phagocytosed by macrophages but have an improved safety profile, are currently entering clinical trials (46). Future studies have to show if ferumoxytol loading of macrophages in humans will allow translational applications of our approach. In addition, we did not prove the origin of the iron oxide–loaded macrophages that migrated into the MASIs. Owing to the close proximity of the MASIs to the bone marrow, it is most likely that bone marrow macrophages migrated into the MASIs. However, we cannot exclude that macrophages from other RES organs, particularly the spleen, may have migrated into our implants. Neither our MR imaging technique nor the histopathologic techniques available to us would have been able to help differentiate between macrophages in the transplant that may have originated from bone marrow and those that may have originated from the spleen or the liver. With regard to differentiating viable from apoptotic MASIs, the origin of the observed macrophage influx may be of academic, but not clinical, importance. Our animal model served as a model for graft failure—that is, primary stem cell apoptosis (eg, that caused by hypoxia)—followed by secondary macrophage influx to clear the dead cells. Our imaging technique would in principle also be applicable to detecting stem cell rejection—that is, primary influx of immune cells into immunogenic transplants (eg, allogeneic transplants) with secondary immune cell–induced death of the transplanted cells. Combinations of our macrophage tracking technique with imaging markers of cell death may help elucidate the timing between transplant death and macrophage influx and may thereby help differentiate graft failure from rejection.

Preloading RES macrophages with intravenous ferumoxytol before stem cell transplantation may provide a new tool for assessing host immune responses to stem cell transplantation noninvasively with MR imaging. Our in vivo macrophage tracking technique may enable us to overcome the bottleneck of diagnosing stem cell transplant failures early after the transplantation, may help us avoid long-term and invasive follow-up studies of lost transplants, and may help in assigning patients with transplant failure to early interventions or alternative treatment options. Potential further applications include comparative in vivo investigations of the host immune response to different stem cell types (human embryonic stem cells, human mesenchymal stem cells, human-induced pluripotent stem cells), comparisons of autologous and allogeneic transplants, investigations of genetically engineered stem cells, comparisons of different scaffolds and growth factors, and assessments of demographic effects on stem cell engraftment outcomes. By exploiting novel and immediately clinically applicable imaging techniques as a new, critical tool for monitoring stem cell engraftment outcomes noninvasively in vivo, we anticipate substantially improving and accelerating the development of successful therapies for cartilage regeneration in patients, thereby alleviating long-term disabilities and related costs to our society. Our imaging technique might also be applicable to monitoring immune responses to other stem cell transplants or immune responses to solid-organ transplants.

Acknowledgment: We thank Jennifer Vancil, CCRC, for her help with the creation and editing of the figures for this manuscript.

Disclosures of Potential Conflicts of Interest: **A.K.** No potential conflicts of interest to disclose. **H.N.** No potential conflicts of interest to disclose. **R.G.** No potential conflicts of interest to disclose. **G.L.** No potential conflicts of interest to disclose. **S.L.** No potential conflicts of interest to disclose. **S.M.** No potential conflicts of interest to disclose. **R.C.** No potential conflicts of interest to disclose. **N.D.** No potential conflicts of interest to disclose. **L.P.** No potential conflicts of interest to disclose. **T.F.L.** Financial activities related to the present article: none to disclose. Financial activities not related to the present article: institution receives money from consultancy for Pfizer, Bayer, and Auxillium; institution has grants or grants pending with Lilly and American Medical Systems. Other relationships: none to disclose. **H.E.D.** Financial activities related to the present article: none to disclose. Financial activities not related to the present article: institution has a seed grant for imaging evaluation of a novel USPIO contrast agent with GE Global Research. Other relationships: none to disclose.

References

1. Hunter W. Of the structure and disease of articulating cartilages: 1743. Clin Orthop Relat Res 1995;(317):3–6.
2. Messner K, Maletius W. The long-term prognosis for severe damage to weight-bearing cartilage in the knee: a 14-year clinical and radiographic follow-up in 28 young athletes. Acta Orthop Scand 1996;67(2):165–168.
3. Behrens P, Bitter T, Kurz B, Russlies M. Matrix-associated autologous chondrocyte transplantation/implantation (MACT/MACI): 5-year follow-up. Knee 2006;13(3):194–202.
4. Nejadnik H, Hui JH, Feng Choong EP, Tai BC, Lee EH. Autologous bone marrow-derived mesenchymal stem cells versus autologous chondrocyte implantation: an observational cohort study. Am J Sports Med 2010;38(6):1110–1116.
5. Toma C, Wagner WR, Bowry S, Schwartz A, Villanueva F. Fate of culture-expanded mesenchymal stem cells in the microvasculature: in vivo observations of cell kinetics. Circ Res 2009;104(3):398–402.
6. van der Bogt KE, Schrepfer S, Yu J, et al. Comparison of transplantation of adipose tissue- and bone marrow-derived mesenchymal stem cells in the infarcted heart. Transplantation 2009;87(5):642–652.
7. Krysko DV, Vandenabeele P. From regulation of dying cell engulfment to development of anti-cancer therapy. Cell Death Differ 2008;15(1):29–38.
8. Karabekian Z, Posnack NG, Sarvazyan N. Immunological barriers to stem-cell based cardiac repair. Stem Cell Rev 2011;7(2):315–325.
9. Dupont KM, Sharma K, Stevens HY, Boerckel JD, García AJ, Guldberg RE. Human stem cell delivery for treatment of large segmental bone defects. Proc Natl Acad Sci U S A 2010;107(8):3305–3310.
10. Lyons FG, Al-Munajjed AA, Kieran SM, et al. The healing of bony defects by cell-free collagen-based scaffolds compared to stem cell-seeded tissue engineered constructs. Biomaterials 2010;31(35):9232–9243.
11. Pei M, He F, Boyce BM, Kish VL. Repair of full-thickness femoral condyle cartilage defects using allogeneic synovial cell-engineered tissue constructs. Osteoarthritis Cartilage 2009;17(6):714–722.
12. Radice M, Brun P, Cortivo R, Scapinelli R, Battaliard C, Abatangelo G. Hyaluronan-based biopolymers as delivery vehicles for bone-marrow-derived mesenchymal progenitors. J Biomed Mater Res 2000;50(2):101–109.
13. Chen L, Tredget EE, Wu PY, Wu Y. Paracrine factors of mesenchymal stem cells recruit macrophages and endothelial lineage cells and enhance wound healing. PLoS One 2008;3(4):e1886.
14. Abdel-Hamid M, Hussein MR, Ahmad AF, Elgezawi EM. Enhancement of the repair of meniscal wounds in the red-white zone (middle third) by the injection of bone marrow cells in canine animal model. Int J Exp Pathol 2005;86(2):117–123.
15. Luong-Van E, Grøndahl L, Song S, Nurcombe V, Cool S. The in vivo assessment of a novel scaffold containing heparan sulfate for tissue engineering with human mesenchymal stem cells. J Mol Histol 2007;38(5):459–468.
16. Koh TJ, DiPietro LA. Inflammation and wound healing: the role of the macrophage. Expert Rev Mol Med 2011;13:e23.
17. Distler JH, Huber LC, Gay S, Distler O, Pisetsky DS. Microparticles as mediators of cellular cross-talk in inflammatory disease. Autoimmunity 2006;39(8):683–690.
18. Lauber K, Bohn E, Kröber SM, et al. Apoptotic cells induce migration of phagocytes via caspase-3-mediated release of a lipid attraction signal. Cell 2003;113(6):717–730.
19. Soehnlein O, Lindbom L. Phagocyte partnership during the onset and resolution of inflammation. Nat Rev Immunol 2010;10(6):427–439.
20. Metz S, Beer AJ, Settles M, et al. Characterization of carotid artery plaques with USPIO-enhanced MRI: assessment of inflammation and vascularity as in vivo imaging biomarkers for plaque vulnerability. Int J Cardiovasc Imaging 2011;27(6):901–912.
21. Simon GH, von Vopelius-Feldt J, Fu Y, et al. Ultrasmall supraparamagnetic iron oxide-enhanced magnetic resonance imaging of antigen-induced arthritis: a comparative study between SHU 555 C, ferumoxtran-10, and ferumoxytol. Invest Radiol 2006;41(1):45–51.
22. Nedopil A, Klenk C, Kim C, et al. MR signal characteristics of viable and apoptotic human mesenchymal stem cells in matrix-associated stem cell implants for treatment of osteoarthritis. Invest Radiol 2010;45(10):634–640.
23. Nedopil AJ, Mandrussow LG, Daldrup-Link HE. Implantation of ferumoxides labeled human mesenchymal stem cells in cartilage defects. J Vis Exp 2010;(38). pii: 1793.
24. Saldanha KJ, Doan RP, Ainslie KM, Desai TA, Majumdar S. Micrometer-sized iron oxide particle labeling of mesenchymal stem cells for magnetic resonance imaging-based monitoring of cartilage tissue engineering. Magn Reson Imaging 2011;29(1):40–49.
25. Sutton EJ, Henning TD, Boddington S, et al. In vivo magnetic resonance imaging and optical imaging comparison of viable and nonviable mesenchymal stem cells with a bifunctional label. Mol Imaging 2010;9(5):278–290.
26. Coyne DW. Ferumoxytol for treatment of iron deficiency anemia in patients with chronic kidney disease. Expert Opin Pharmacother 2009;10(15):2563–2568.
27. Laurent S, Forge D, Port M, et al. Magnetic iron oxide nanoparticles: synthesis, stabilization, vectorization, physicochemical characterizations, and biological applications. Chem Rev 2008;108(6):2064–2110.
28. Ning H, Lin G, Lue TF, Lin CS. Neuron-like differentiation of adipose tissue-derived stromal cells and vascular smooth muscle cells. Differentiation 2006;74(9-10):510–518.
29. Chang SW, Chou SF, Chuang JL. Mitomycin C potentiates ultraviolet-related cytotoxicity in corneal fibroblasts. Cornea 2008;27(6):686–692.
30. Arinzeh TL, Peter SJ, Archambault MP, et al. Allogeneic mesenchymal stem cells regenerate bone in a critical-sized canine segmental defect. J Bone Joint Surg Am 2003;85-A(10):1927–1935.
31. Azoulay R, Olivier P, Baud O, et al. USPIO (Ferumoxtran-10)-enhanced MRI to visualize reticuloendothelial system cells in neonatal rats: feasibility and biodistribution study. J Magn Reson Imaging 2008;28(4):1046–1052.
32. Tsuchiya K, Nitta N, Sonoda A, et al. Histological study of the biodynamics of iron oxide nanoparticles with different diameters. Int J Nanomedicine 2011;6:1587–1594.
33. Oghabian MA, Gharehaghaji N, Amirmohseni S, Khoei S, Guiti M. Detection sensitivity of lymph nodes of various sizes using USPIO nanoparticles in magnetic resonance imaging. Nanomedicine 2010;6(3):496–499.
34. Daldrup HE, Link TM, Blasius S, et al. Monitoring radiation-induced changes in bone marrow histopathology with ultra-small superparamagnetic iron oxide (USPIO)-enhanced MRI. J Magn Reson Imaging 1999;9(5):643–652.
35. Daldrup-Link HE, Rummeny EJ, Ihssen B, Kienast J, Link TM. Iron-oxide-enhanced MR imaging of bone marrow in patients with non-Hodgkin's lymphoma: differentiation between tumor infiltration and hypercellular bone marrow. Eur Radiol 2002;12(6):1557–1566.

36. Senéterre E, Weissleder R, Jaramillo D, et al. Bone marrow: ultrasmall superparamagnetic iron oxide for MR imaging. Radiology 1991;179(2):529–533.

37. Simon GH, Bauer J, Saborovski O, et al. T1 and T2 relaxivity of intracellular and extracellular USPIO at 1.5T and 3T clinical MR scanning. Eur Radiol 2006;16(3):738–745.

38. Weissleder R, Elizondo G, Wittenberg J, Rabito CA, Bengele HH, Josephson L. Ultrasmall superparamagnetic iron oxide: characterization of a new class of contrast agents for MR imaging. Radiology 1990;175(2):489–493.

39. Bierry G, Jehl F, Boehm N, Robert P, Dietemann JL, Kremer S. Macrophage imaging by USPIO-enhanced MR for the differentiation of infectious osteomyelitis and aseptic vertebral inflammation. Eur Radiol 2009;19(7):1604–1611.

40. Trivedi RA, U-King-Im JM, Graves MJ, et al. In vivo detection of macrophages in human carotid atheroma: temporal dependence of ultrasmall superparamagnetic particles of iron oxide-enhanced MRI. Stroke 2004;35(7):1631–1635.

41. Henning TD, Gawande R, Khurana A, et al. Magnetic resonance imaging of ferumoxide-labeled mesenchymal stem cells in cartilage defects: in vitro and in vivo investigations. Mol Imaging 2011;11(3):197–209.

42. Henning TD, Wendland MF, Golovko D, et al. Relaxation effects of ferucarbotran-labeled mesenchymal stem cells at 1.5T and 3T: discrimination of viable from lysed cells. Magn Reson Med 2009;62(2):325–332.

43. Kraitchman DL, Kedziorek DA, Bulte JW. MR imaging of transplanted stem cells in myocardial /9*-infarction. Methods Mol Biol 2011;680:141–152.

44. van Buul GM, Kotek G, Wielopolski PA, et al. Clinically translatable cell tracking and quantification by MRI in cartilage repair using superparamagnetic iron oxides. PLoS One 2011;6(2):e17001.

45. Corot C, Petry KG, Trivedi R, et al. Macrophage imaging in central nervous system and in carotid atherosclerotic plaque using ultrasmall superparamagnetic iron oxide in magnetic resonance imaging. Invest Radiol 2004;39(10):619–625.

46. Daldrup-Link HE, Golovko D, Ruffell B, et al. MRI of tumor-associated macrophages with clinically applicable iron oxide nanoparticles. Clin Cancer Res 2011;17(17):5695–5704.